A Study of Electrical Properties in Bismuth Thin Films

Chun Yang
Centenary College of Louisiana
Shreveport, LA 71104

Physics REU Summer 2008
University of Florida
Gainesville, FL 32611

When bismuth is grown in thin-film geometry, it exhibits unusual behavior as compared to its bulk properties. A lack of the large magnetoresistance effect is noted, as well as a decreasing resistivity versus temperature trend as related to film thickness that saturates at low temperatures. Also of interest is the potential existence of resonant tunneling due to impurity centers at the grain boundaries. These effects are shown through standard four-terminal measurements of a Hall-bar film grown on sapphire substrates wetted with calcium fluoride.

Introduction

In the study of the physical properties of elements, semimetals have attracted much attention due to their unique properties of perfect compensation—or the exact equality in numbers of free electrons and holes—and a low scattering rate. These characteristics give rise to a temperature and magnetic field dependence of the resistance. This magnetic field effect, otherwise known as the magnetoresistance, in semimetals is known to be very high [1]. These bulk characteristics make semimetals useful for magnetic field sensing applications. Thus the semimetal, bismuth, has already been the subject of extensive study.

Studies of thin-film bismuth, in comparison, have often been hampered by the difficulty involved in sample growth. Due to its high surface tension, the initial islands that form during thin-film growth of bismuth through thermal evaporation tend to ball up into separate grains rather than joining smoothly. The focus of this project was to grow bismuth thin films of sufficient quality and then to examine their electric properties as a function of temperature and magnetic field strength. Thin films, being a restricted 2D geometry, are noted for unusual physical phenomena as compared to bulk properties. Therefore, it is of interest to compare the thin-film properties of bismuth with those of the bulk. The films were grown in a Hall-bar geometry due to the convenience of being able to measure longitudinal and transverse voltages simultaneously.

The Hall Effect and Hall-Bar Geometry

As arranged in Fig. 1, current is sourced through the bar-shaped film in the longitudinal direction.

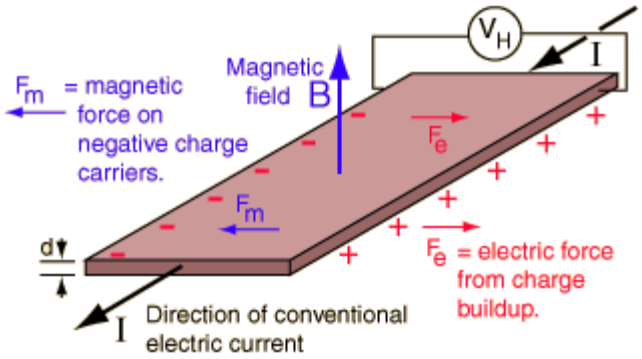

Figure 1. The Hall effect in a thin film. [Source: C. Nave, *Hyperphysics.*]

When applying a magnetic field in the direction shown, a Lorentz force causes a transient transverse current. As electrons are mutually repulsive, they cannot all cluster at the edge. This results in a concentration gradient of the electron carrier density in the film as electron flow again proceeds in the longitudinal direction. The potential difference that arises from the gradient is known as the Hall-effect voltage. Thus, the Hall-effect voltage is directly related to the carrier density of the material. Eq. (1) expresses this relationship with I the current, B the magnetic field, n the carrier density of the electrons, e the charge of an electron and d the thickness of the film:

$$V_H = \frac{I \cdot B}{n \cdot e \cdot d} \ . \qquad (1)$$

In addition, the sign of this voltage gives an indication of whether electrons or holes carry the flow of charge. This would indicate the sign of the charges (electron or holes) participating in the current flow in a material under an applied magnetic field. To derive the value of the carrier density, both sides of Eq. (1) are first divided by the current I to get the transverse resistance as a function of the magnetic field multiplied by $1/n \cdot e \cdot d$. Dividing both sides of this by B then leaves the $1/n \cdot e \cdot d$ factor as a function of the slope of the resistance versus magnetic field. This can then

be solved for n the carrier density:

$$n = \frac{1}{\frac{\Delta R}{\Delta B} \cdot e \cdot d} \qquad (2)$$

with the charge of the electron a known value and d the film thickness and the slope of R vs. B being measureable values.

The Hall-bar geometry as shown in Fig. 2 has two pairs of contact legs. The value of this shape is that the legs reduce the misalignment of the leads applied to the film for measurement purposes. Moreover, wires pressed onto these contacts will not damage the central bar of the film. These wires can then be hooked up to devices that measure the longitudinal (V_{xx}) and transverse (V_{xy}) voltages while sourcing current through the ends. The transverse voltage measured is the Hall-effect voltage. Meanwhile, the resistance along the longitudinal axis measured against the change in the magnetic field gives the magnetoresistance of the film.

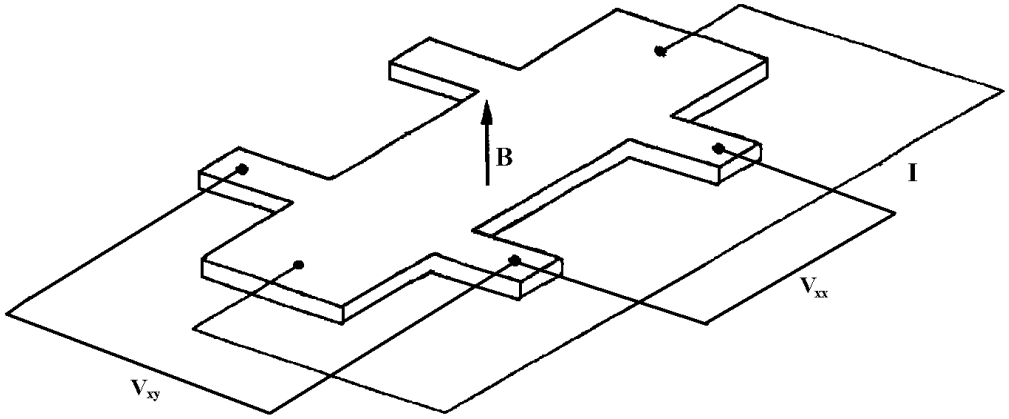

Figure 2. Hall-bar geometry. Current is sourced through the ends while the longitudinal and transverse (or Hall-effect) resistances are measured.

Grain Boundaries and Resonant Tunneling

Due to the existence of grain boundaries in growing thin films by thermal evaporation, the resistivity increases when compared to single-crystal bulk bismuth. The inelastic tunneling of electrons through these grain boundaries is thermally assisted except at low temperatures where the tunneling probability, hence the resistance, is independent of temperature [3].

The existence of resonant tunneling depends on the presence of one or more impurity centers at a grain boundary. Resonant tunneling, as depicted in Fig. 3, causes a detectable change in the linear relationship between conductivity and temperature. A linear relationship between conductivity and $T^{4/3}$ is an indication of resonant tunneling due to a single impurity center. In addition, a linear relation for a power greater than 4/3 is an indication of multiple impurity centers at the grain boundary [4].

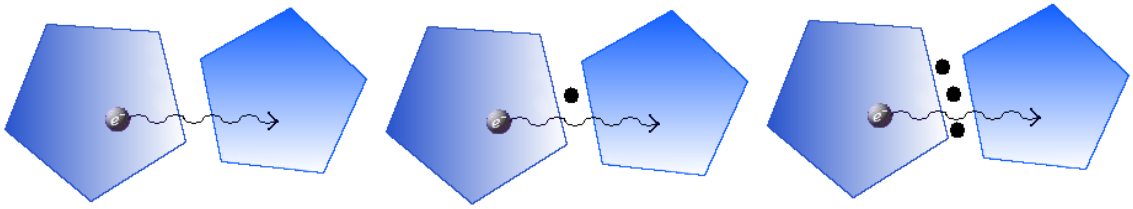

(a) (b) (c)

Figure 3. Resonant tunneling at a grain boundary in the presence of (a) no impurity centers (b) a single impurity center (c) multiple impurity centers.

Experimental

The thin films in this study were grown by thermal evaporation. We ran a high current through a tungsten "boat" (the source) containing the substance being grown, causing it to evaporate up towards a substrate facing down. Under the proper temperature, pressure, and surface geometry conditions, the material then deposits upon this substrate. The substrate holder was connected to a heater in order to grow samples that required higher temperatures. We used a diffusion vacuum pump to reduce the pressure in the evaporator chamber to a range of $10^{-6} \sim 10^{-7}$ Torr. This reduced the density of the air molecules in the chamber, increasing the mean free path that the atoms of the source material could travel between the boat and the substrate. To monitor the rate and amount of material grown, we placed a quartz crystal monitor next to the substrate. A shutter was used to cover the substrate until the crystal monitor detected the desired growth rate.

We first grew plain bismuth thin films upon sapphire substrates that came from precut wafers of rectangular shape. Due to the presence of dust particles on the substrates, we had to clean them thoroughly through sonication with a Branson 1210. We heated the substrate holder to 900 K and then grew a layer of calcium fluoride of varying thickness to "wet" the surface of the substrate. CaF_2 has a high adhesive force that facilitates the growth of bismuth, yielding a smoother film. Initially, we investigated growing bismuth films at varying temperatures. As we found bismuth would not deposit on the substrate at high temperatures such as 500 K, subsequent samples of bismuth film were grown at room temperature.

Then we grew bismuth films in the above-mentioned Hall-bar geometry by positioning a high-precision shaped shadow mask over the substrate after CaF_2 deposition. We made three samples with thicknesses of 1500, 500, and 100 counts at a rate of 5-7 counts per second. The system was then vented with argon gas to minimize oxidization of the film prior to measurement. A Profileometer measured these films to be of 2200 (Bismuth 1), 700 (Bismuth 2), and 140 (Bismuth 3) angstroms thickness, respectively. A second 2200 angstrom sample was made and then annealed in a constant flood of argon gas at around 530 K for four hours.

A Physical Properties Measurement System (PPMS) was used for studying properties such as resistance versus temperature and magnetoresistance. We attached our samples to a specially designed puck for placement into the PPMS. The contacts for the voltage measurements and the source current of the Hall bars were connected with gold wires pressed with indium to the contacts on the puck. The PPMS is capable of sweeping between 1.8 and 300 K temperature and -7 to 7 T fields while taking measurements through LabView on a computer. We used an LR 700 to source current through the film at 16 Hz. This device automatically calculates the resistances from the voltage measurements due to the current sourced.

Measurements were made of the magnetoresistance, Hall resistance, and longitudinal resistance versus temperature. We then used an Atomic Force Microscope (AFM) to examine the surface morphology of the 2200 Å and 700 Å samples.

Results

Sheet Resistivity/Conductivity versus Temperature

The rectangle between the four terminal contact legs of the Hall bars is twice as long as it is wide. Therefore, we calculated the sheet resistivity (ρ) for the samples by dividing the measured longitudinal resistance by two and multiplying by the film thickness. Fig. 4 shows the temperature dependence of ρ from 2 K to 300 K. The decreasing relation between T and ρ is a characteristic of insulator behavior. However, the saturation of the resistivity at low temperatures is an indication that these films are not purely insulating and that temperature-independent tunneling is most likely dominating. The annealed sample was created much later the than the other three samples and shows the lowest resistivity trend of the entire set.

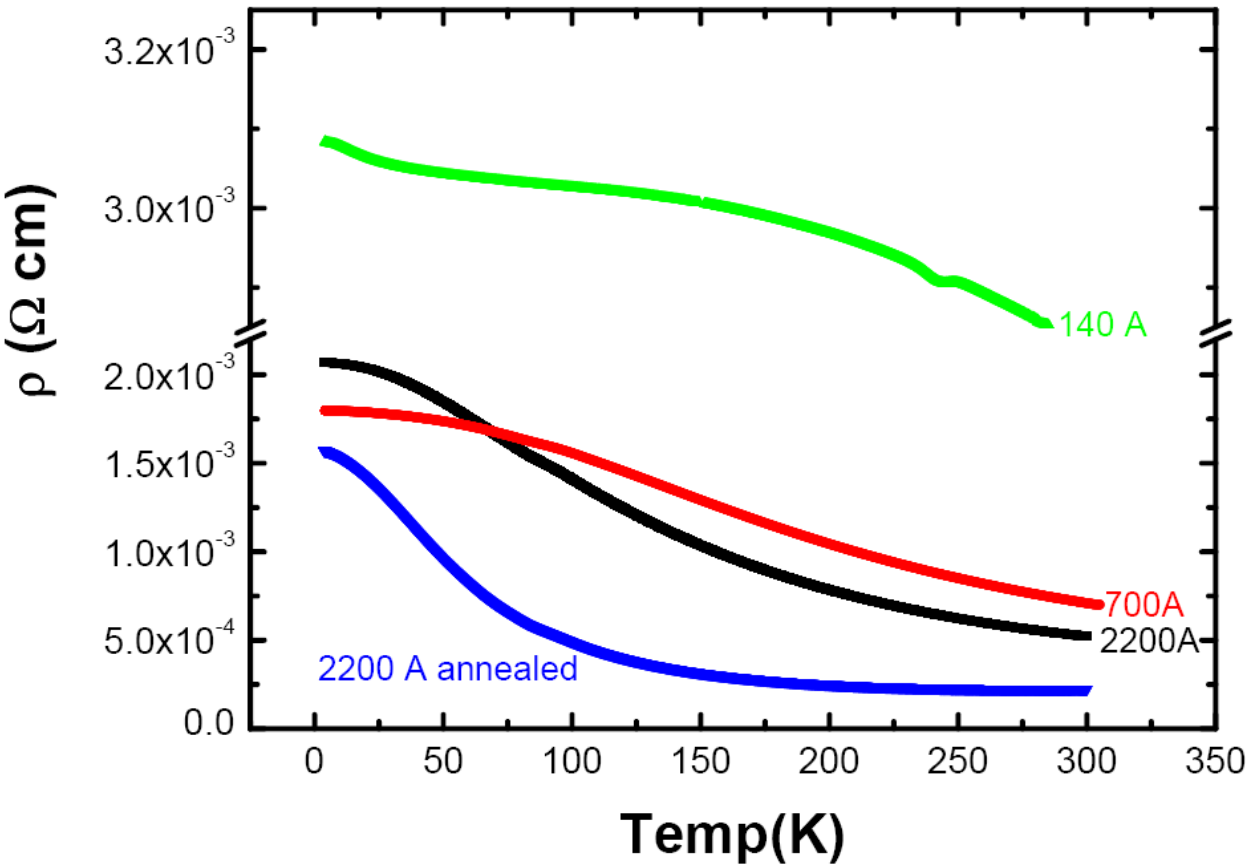

Figure 4. Combined resistivity vs. temperature for bismuth samples. Bismuth 3 (140 Å) shows the highest overall resistivity, while Bismuth 1 (2200 Å) initially shows a higher resistivity than Bismuth 2 (700 Å) at lower temperatures. The annealed 2200 Å sample has the lowest overall resistivity.

Figs. 5, 6, and 7 show the sheet conductivity (σ), or the inverse resistivity, of the three samples as a function of temperature. Figs. 5 and 6 also show a plot of σ vs. $T^{4/3}$. Clearly, the graph of σ vs. T shows more linearity than the σ vs. $T^{4/3}$ graph for Bismuth 1. In Bismuth 2, however, the σ vs. $T^{4/3}$ plot is more linear, which demonstrates a resonant tunneling effect due to a single impurity. Using OriginPro and a power rule fitting, we found the conductivity of Bismuth 3 to be linear against an order of $T^{2.86}$. This result indicates a resonant tunneling mechanism due to multiple impurity centers. The cause of the "bump" at around 250 K for Bismuth 3 is unknown.

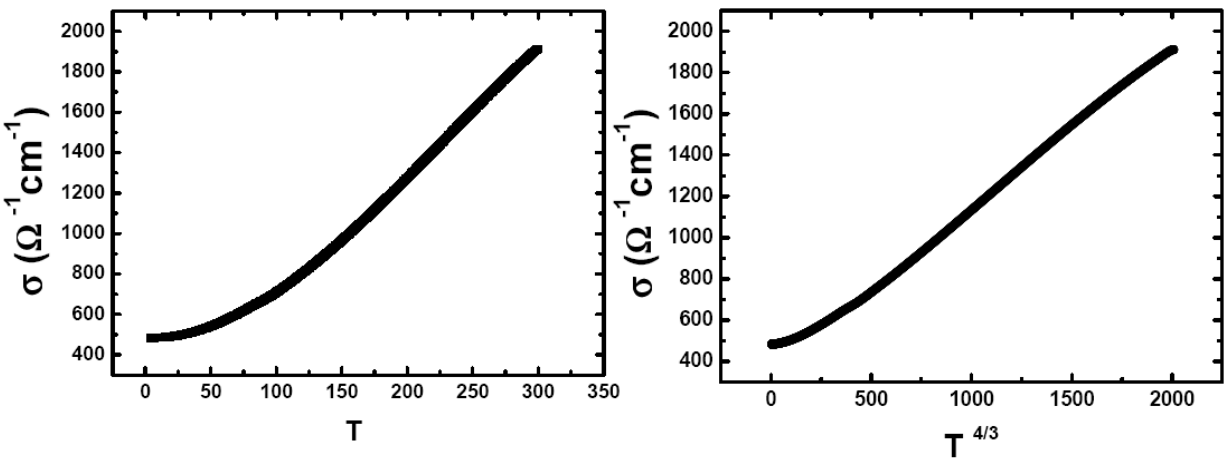

Figure 5. Conductivity vs. Temperature (K) and $T^{4/3}$ for Bismuth 1 (2200Å).

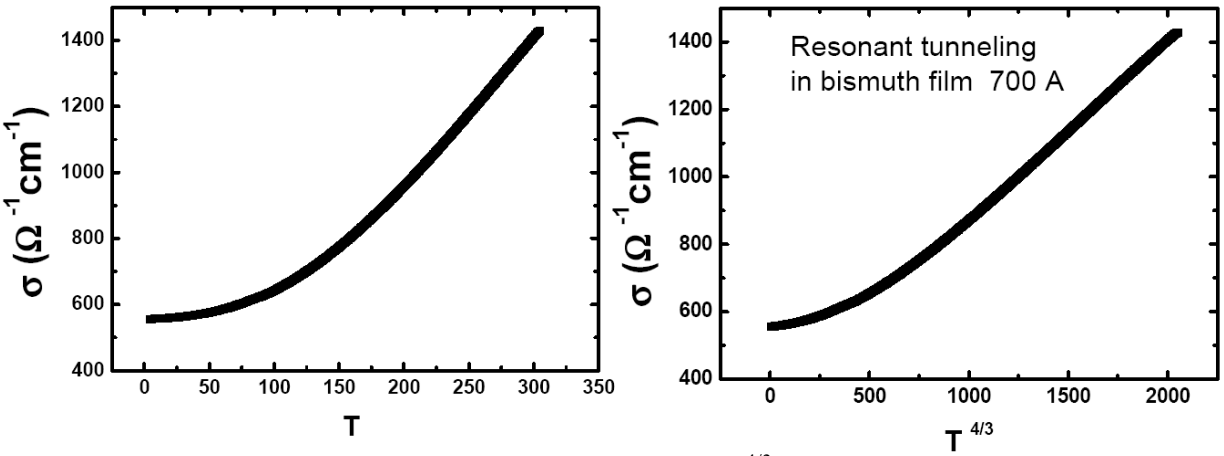

Figure 6. Conductivity vs. temperature T (in K) and vs. $T^{4/3}$ for Bismuth 2 (700Å). The linear dependence of σ vs. $T^{4/3}$ is an indication of resonant tunneling due to a single impurity.

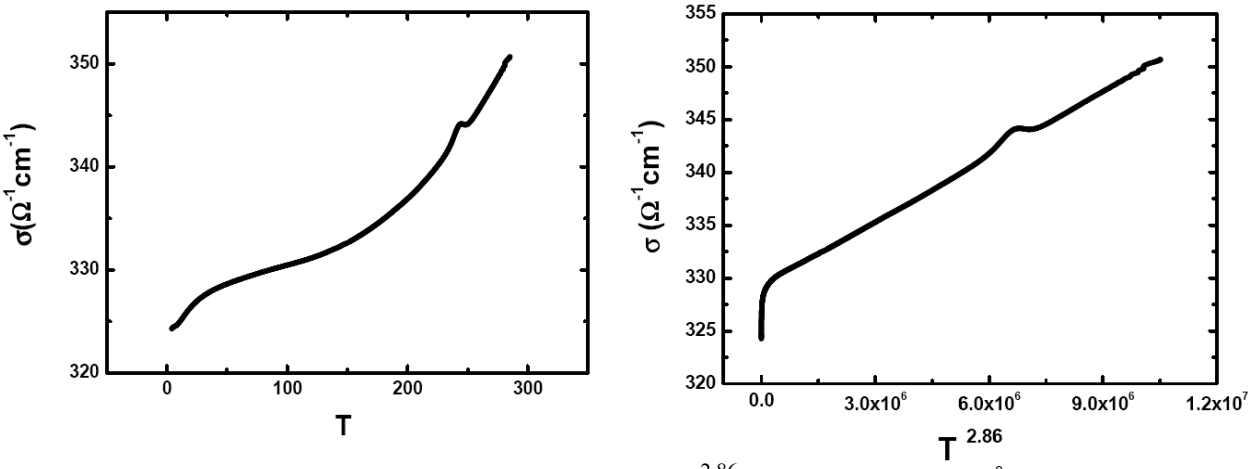

Figure 7. Conductivity vs. temperature T (in K) and $T^{2.86}$ for Bismuth 3 (140Å). The linear dependence of a power of T greater than 4/3 is an indication of resonant tunneling due to multiple impurity centers.

Hall-Effect Resistance and Carrier Density

We measured the transverse resistance, or the Hall-effect resistance, while sweeping the sample with a magnetic field between positive and negative. This allowed us to correct for the small unavoidable misalignment between the Hall leads for the V_{xy} measurement. This misalignment causes a fraction of the longitudinal resistance to be measured along with the transverse potential. We then calculated the Hall resistance using Eq. (3) (the relationship between voltages being the same as the relationship between resistances):

$$V_H = \frac{V_{xy}(B) - V_{xy}(-B)}{2} . \qquad (3)$$

Figs. 8, 9, and 10 show the Hall-effect resistance versus magnetic field for Bismuth 1, 2, and 3 respectively. The discontinuous points in the plots are anomalous. We conducted measurements while sweeping the magnetic field between -7 T and 7 T at differing temperatures for Bismuth 3 as shown in Fig. 10 (the data for 4.2 K and 5 K overlap very closely). However, due to time constraints in the access to the PPMS, we conducted these sweeps at 4.2 K for Bismuth 1 and 2 at a lower resolution and magnetic field range. The annealed sample was analyzed due to the sudden availability of the PPMS for one day, so we have no Hall data (and thus later no electron concentration data) available for this report.

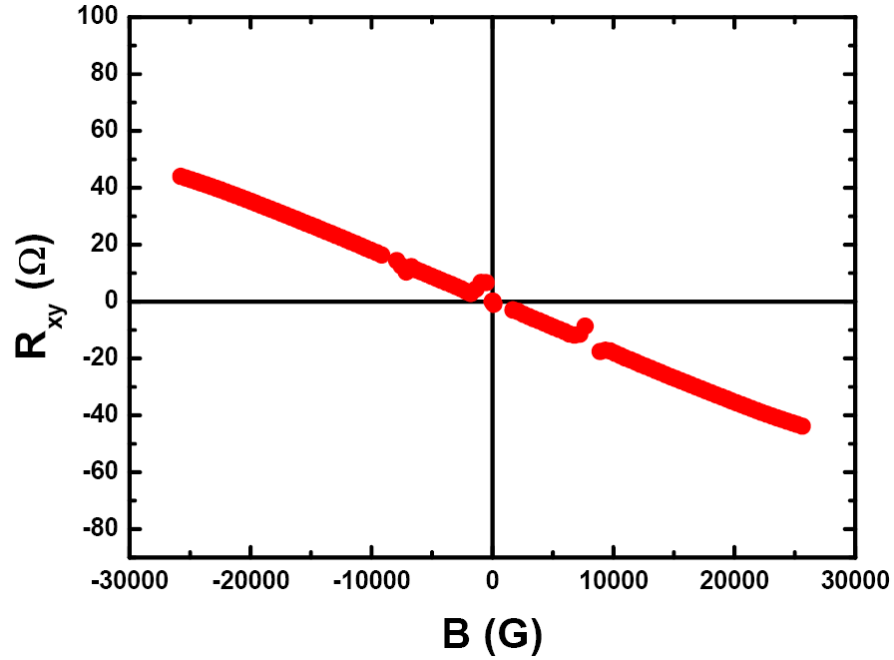

Figure 8. Hall-effect resistance vs. magnetic field for Bismuth 1 (T = 4.2 K).

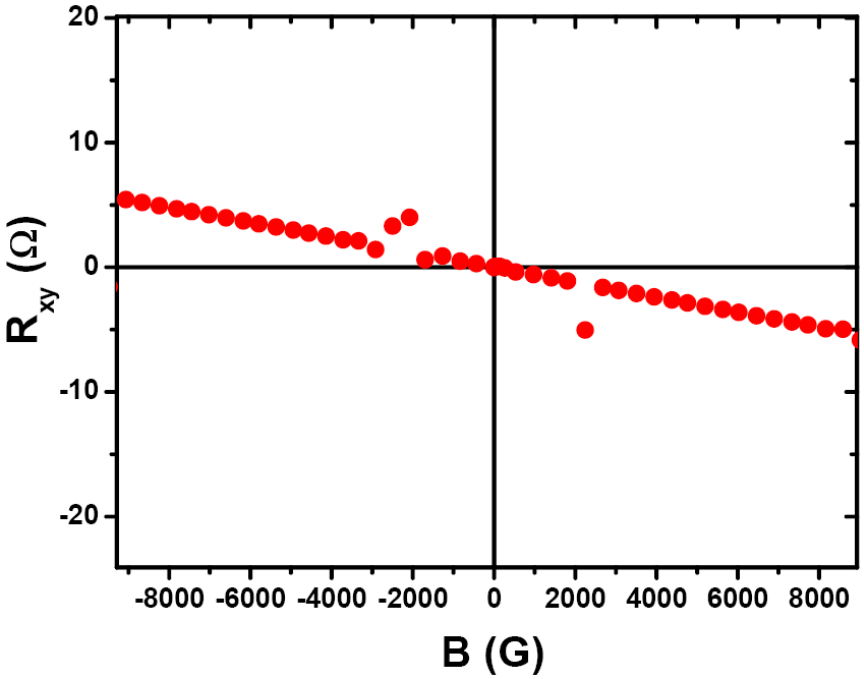

Figure 9. Hall-effect resistance vs. magnetic field for Bismuth 2 (T = 4.2 K).

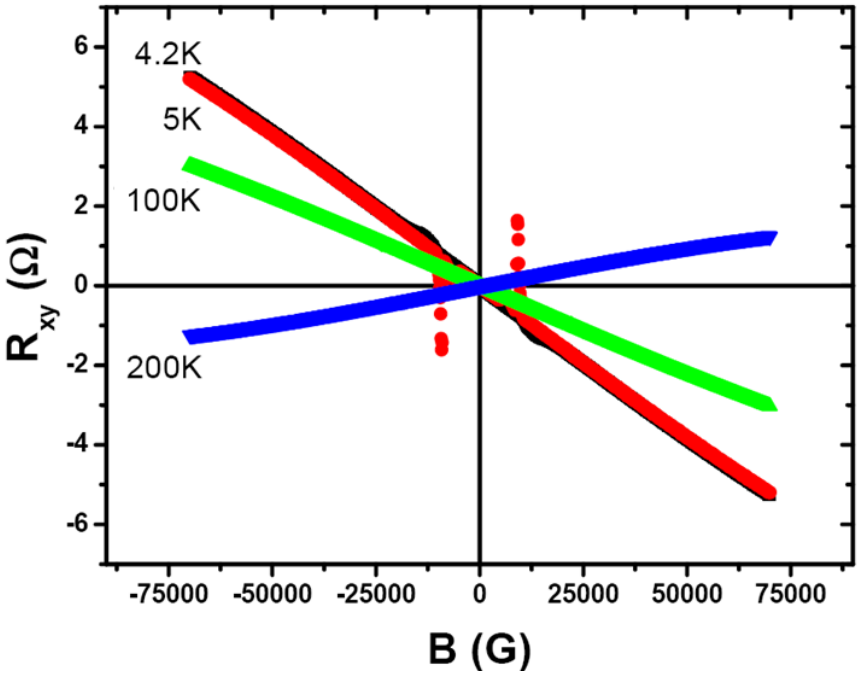

Figure 10. Hall-effect resistance vs. magnetic field for Bismuth 3. With increasing temperature, the slope of the Hall-effect resistance shifted from positive to negative. The 4.2 K and 5 K plots have near perfect overlaps.

We extracted the slopes of the *R* vs. *B* plots from Figs. 8, 9, and 10 and solved for the carrier density using Eq. (2). The carrier density values at 4.2 K were then plotted against film thickness in Fig. 11.

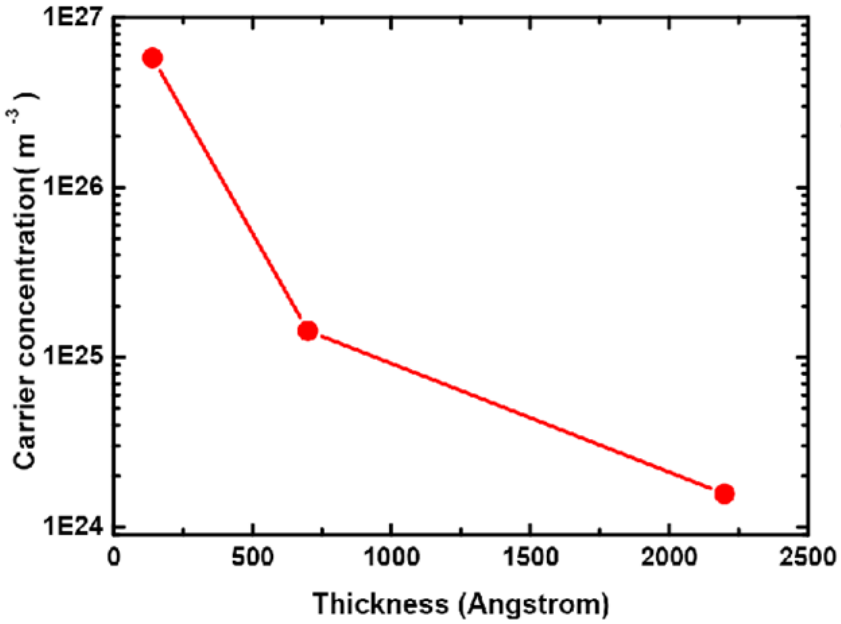

Figure 11. Electron carrier density as a function of thickness of Bi films at 4.2 K.

Table I lists the data points of carrier concentration versus temperature of Bismuth 3. Of note is the positive carrier density at 200 K. This result shows the existence of a shift between the dominance of electrons and holes with a change in temperature.

Table I. Carrier concentrations of Bismuth 3 (140 Å)

temp. (K)	carrier concentration (m^{-3})
4.2	-5.82×10^{26}
5	-5.91×10^{26}
100	-1.01×10^{27}
200	2.36×10^{27}

Due to the same time limitations for the Hall-effect measurements, we took data for the magnetoresistance of the Bismuth 3 sample and the annealed sample only. The change in the longitudinal resistance for Bismuth 3 over a range of -7 to 7 Tesla (-70 to 70 kGauss) at 4.2 K is plotted in Fig. 12. This same plot is made in Fig. 13 for the annealed sample. Bismuth 3 shows a notably smaller magnetoresistance effect than that in bulk bismuth, implying that scattering at grain boundaries of the film sharply limits the mean free path, and thus the magnetoresistance. The magnetoresistance for the annealed sample, however, shows a change of about 170% from zero to 7 Tesla.

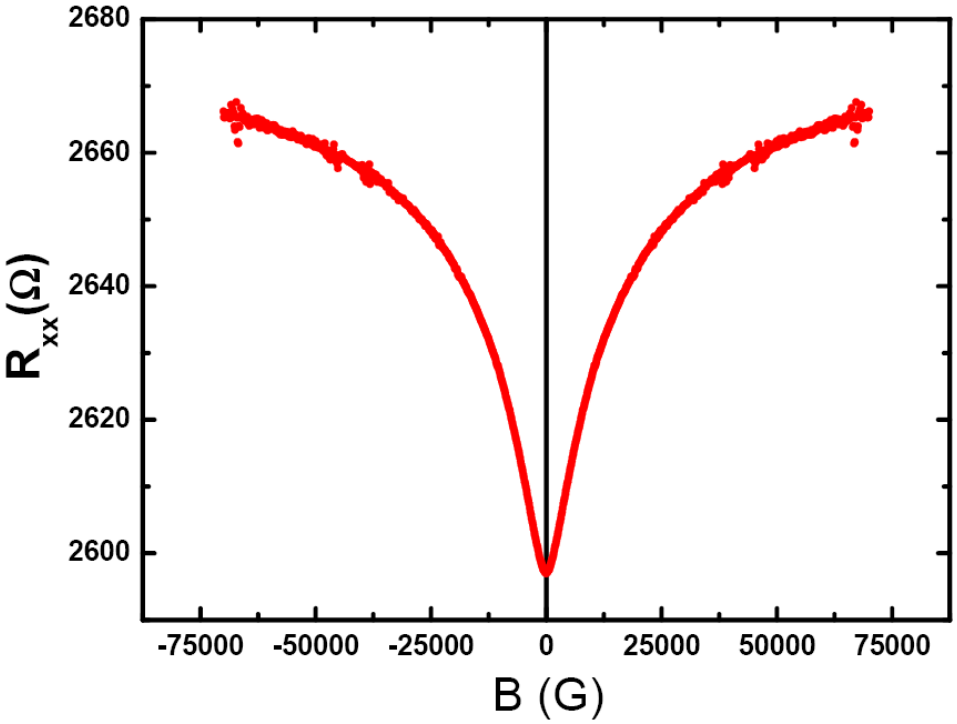

Figure 12. Magnetoresistance of Bismuth 3 (T = 4.2 K).

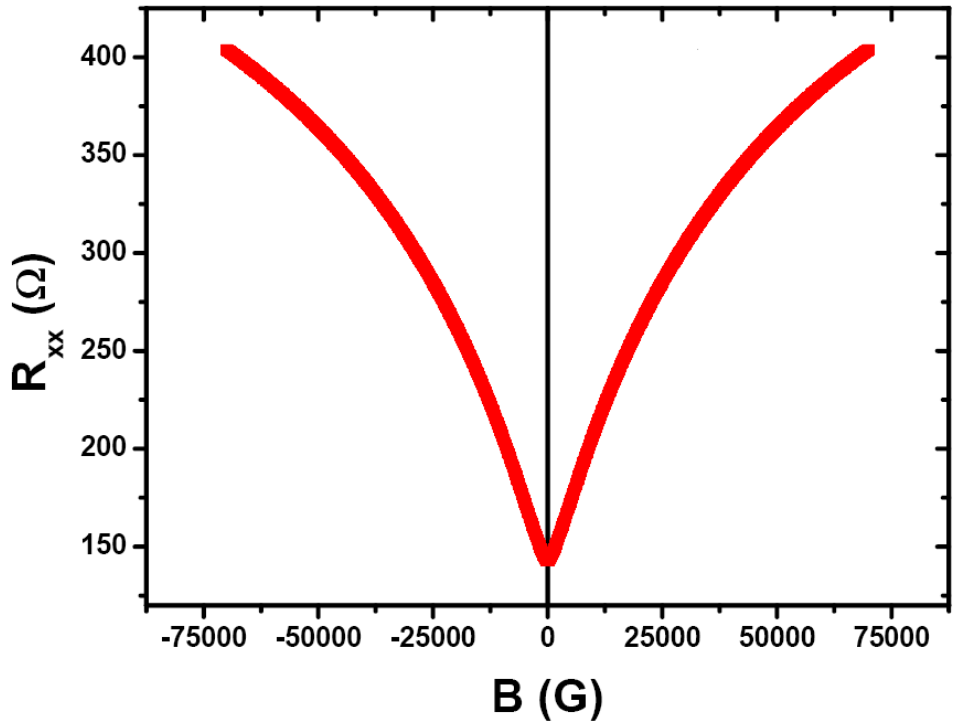

Figure 13. Magnetoresistance of annealed bismuth (T = 4.2 K).

Morphology

We performed AFM scans of the surfaces of the Bismuth 1 and 2 samples shown in Figs. 14 and 15, respectively. The root-mean-square (RMS) roughness of Bismuth 1 was very small at 35 Å. Bismuth 2's RMS roughness of 123 Å was still of sufficient quality for our purposes. All films grown appeared extremely smooth to the eye and had a metallic gleam. Bismuth 3 was unavailable for AFM scanning at the time of measurement.

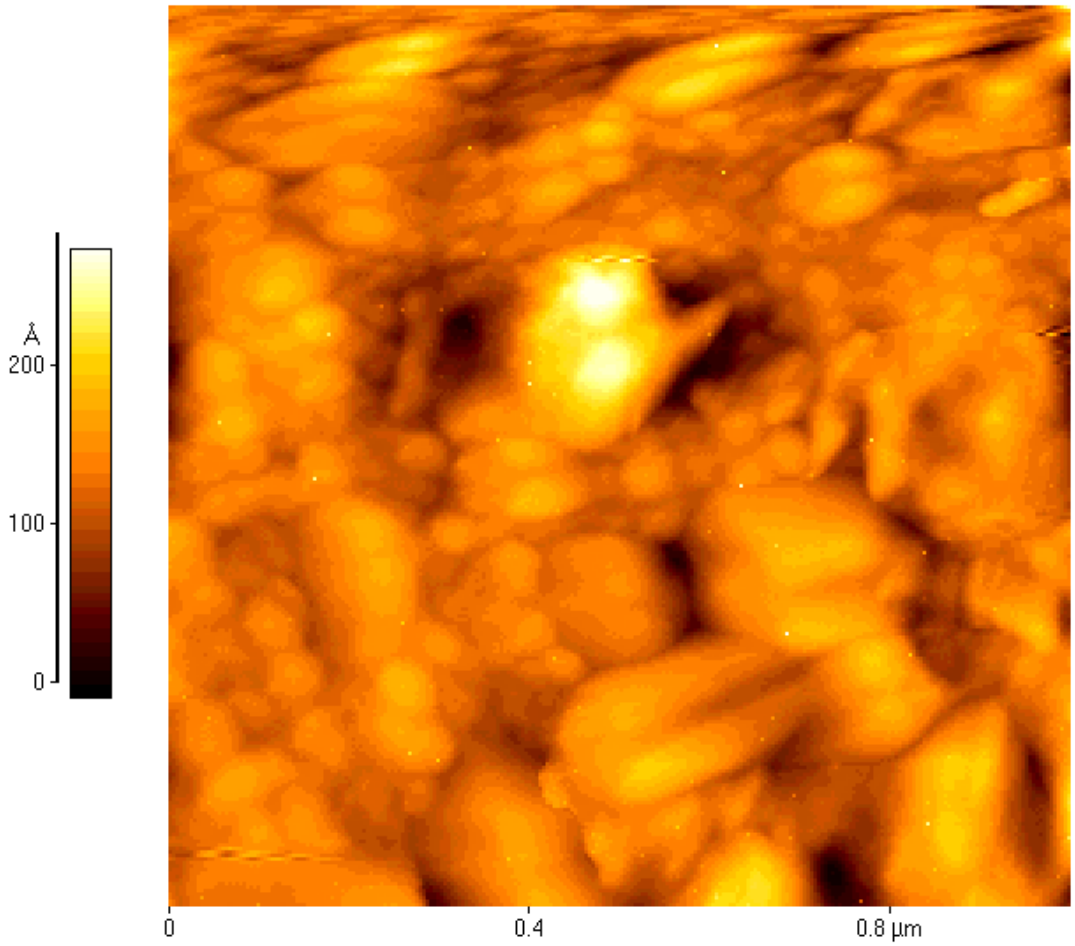

Figure 14. AFM image of Bismuth 1 (RMS roughness 35 Å).

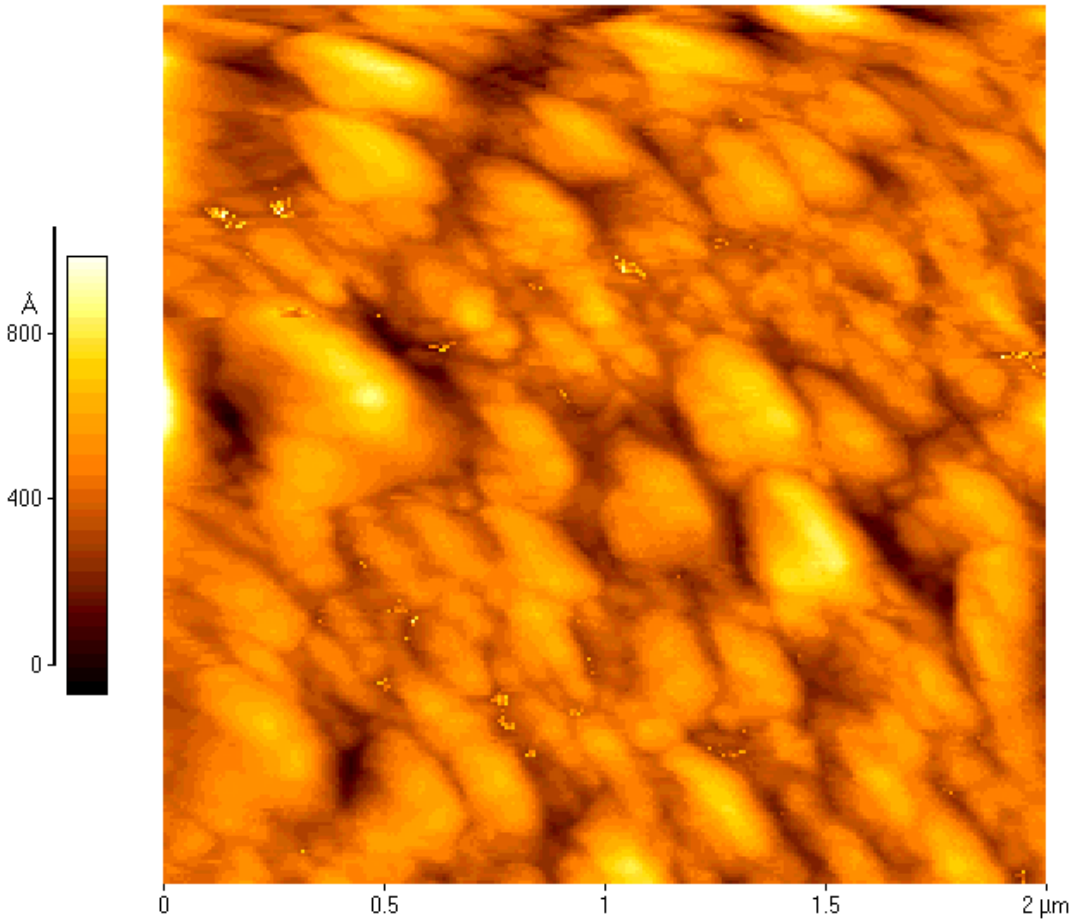

Figure 15. AFM image of Bismuth 2 (RMS roughness of 123 Å)

Concluding Thoughts

After the initial problems with the temperature for bismuth deposition, we achieved a consistent quality for the bismuth films by first growing a CaF_2 layer and growing the bismuth at room temperature. It is interesting to note the lack of an observed magnetoresistance effect of large (10^5) magnitude in the Bismuth 3 sample. This can be attributed to the small-grain-size polycrystalline films grown by using vapor deposition techniques [5]. The annealing affect unexpectedly provided a much greater shift in the magnetoresistance; this shows a much more bulk-like behavior, implying fewer grains existed in the film (yet still not achieving the large effect in bulk). Better methods for film deposition would increase the time required for this

project beyond the scope of an REU project. Nonetheless, the existence of the grain boundaries due to the polycrystalline structure allows for some interesting study.

The resonant tunneling mechanism in Bismuth 2 and 3 cannot exist in single-crystal bulk bismuth, as there are no grain boundaries in a single-crystal formation. While the bumps and discontinuities in Figures 7-10 are unexpected, they do not greatly disturb the overall trends observed in these measurements. Of great interest is the resistivity versus temperature data in Fig. 4. Pure bulk bismuth has a metallic temperature-dependent behavior in a zero magnetic field and transitions to an insulating behavior in a nonzero magnetic field with increasing resistivity with the increase in magnetic field [6]. The decrease of resistivity as a function of thickness in Fig. 4 of thin-film bismuth resembles this insulating behavior inverted (with the annealed sample displaying an even lower resistivity trend), yet this is at a zero magnetic field. As per the magnetoresistance data, this seems to imply decreasing resistivity means a more homogenous film was grown. This makes sense as single crystal bulk bismuth behaves in a metallic manner.

Further work could include a more detailed exploration of the potential resonant tunneling observed and a more detailed analysis of the magnetoresistance at a greater strength and resolution. Our project was hampered in this regard due to the limited availability of the PPMS analysis system. The annealed data came from a sudden unexpected free day in the PPMS schedule. Also, a slower rate of growth for the bismuth films may lead to more bulk-like behavior, which would be promising for electric field gating purposes. In addition, the reason behind the anomalous “bumps” in our various figures needs addressing.

Acknowledgements

I would like to acknowledge the organizers of the REU program at the University of Florida, in particular Dr. Kevin Ingersent and Kristin Nichola, for providing an enjoyable experience for the summer. I would also like to thank Dr. Art Hebard for providing me with a stimulating learning environment and for his advisement. Especially, I would like to thank the graduate students of the Hebard lab group, in particular Rajiv Misra, Siddhartha Ghosh, Ritesh Das, Sefaattin Tongay, and Patrick Mickel, for their patience and profuse help in this 10-week laboratory experience. Of course, I would like to acknowledge the NSF for funding the REU program.

References

[1] S. G. Bompadre, C. Biagini, D. Maslov, and A. F. Hebard, Phys. Rev. B **64**, 07310 (2001).

[2] C. Nave, *Hyperphysics*, (http://hyperphysics.phy-astr.gsu.edu/hphys.html).

[3] J. J. G. Kelly IV, Du Xu, S. Echols, D. L. Maslov, and A. F. Hebard, unpublished draft paper.

[4] Yizi Xu, D. Ephron, and M. R. Beasley, Phys. Rev. B **52**, 2843 (1995).

[5] D. E. Beutler and N. Giordano, Phys. Rev. B **38**, 8 (1988).

[6] Xu Du, Shan-Wen Tsai, Dmitrii L. Maslov et al., Phys. Rev. Lett. **94**, 166601 (2005).